Monte Carlo estimates of $\%dd(10)_\mathsf{x}$ for the NPL photon beams

B.R.B. Walters and D.W.O. Rogers
Ionizing Radiation Standards
National Research Council of Canada
Ottawa, K1A OR6

bwalters@irs.phy.nrc.ca
June, 2000

NRCC Report PIRS-0659rev

Abstract

The NPL reports their data for k_Q as a function of TPR_{10}^{20} but they also have measured values of $\%dd(10)$ at SSD's of 120 cm and 118 cm. To compare their measured k_Q data to ours, we require an estimate of $\%dd(10)_\mathsf{x}$ (the photon component of $\%dd(10)$ for a 10×10 cm^2 field at SSD=100 cm). $\%dd(10)_\mathsf{x}$ can be estimated from the measured values of $\%dd(10)$ by multiplying the latter by an electron contamination factor, ϵ and then adding a factor, Δ, to convert from the NPL SSD to SSD=100 cm. We simulate the NPL photon accelerator for various energies and filtrations using the BEAM Monte Carlo code. Depth-dose curves from the simulation are then used to calculate ϵ, and photon spectra from the simulations are input to the computer code DDSPR to calculate Δ. Values of $\%dd(10)$ calculated from BEAM depth-dose curves are within 2.5% of measured values (rms deviation = 1%) while calculated values of TPR_{10}^{20} are within 1% of measurement (rms deviation = 0.4%). We investigate the effect of parallel vs conical incident beams and incident beam spot size and find these have no significant effect on the calculated values of $\%dd(10)$, $\%dd(10)_\mathsf{x}$ and TPR_{10}^{20}. We also simulate a 7% drop in the incident energy. This decreases calculated values of $\%dd(10)$, $\%dd(10)_\mathsf{x}$ and TPR_{10}^{20}, however the effect on TPR_{10}^{20} decreases with increasing energy. In all cases we find that using the lower incident energy makes agreement with experiment worse than when the nominal energy is used, sometimes substantially. We use both the central axis photon spectrum and the photon spectrum over the entire beam field as input to DDSPR. Both spectra give equally good agreeement with BEAM depth-dose results, and the calculated Δ does not depend on which spectrum is used. Once ϵ and Δ are applied to the measured values of $\%dd(10)$ we have an estimate of $\%dd(10)_\mathsf{x}$ for the NPL beams. Using this beam quality specifier, the NPL's measured values of k_Q for the heavily- and lightly-filtered beams are in good agreement with each other whereas plotted as a function of TPR_{10}^{20} they fall on two distinct curves.

Contents

1 Introduction

To allow meaningful comparison of NPL measured k_Q values and those measured at NRC, one needs the beam quality specifier, $\%dd(10)_{\mathsf{x}}$ for the NPL beams. This specifier is defined as the photon component of $\%dd(10)$ for a 10x10 cm^2 field at SSD=100 cm. This specifier is not available for the NPL setup which has a 100 cm^2 beam at an SSD of 118 or 120 cm. This report presents a method of determining $\%dd(10)_{\mathsf{x}}$ for the NPL beams based on detailed Monte Carlo calculations of the NPL accelerator. The results show that if one plots NPL's measured k_Q values as a function $\%dd(10)_{\mathsf{x}}$, then there is no distinction between calibration factors measured in lightly or heavily filtered beams except for the 4 MV lightly-filtered beam. This is consistent with earlier results based on much cruder estimates of the NPL's beams[1].

The method presented depends on detailed Monte Carlo simulations of these beams. We are aware of three previous simulation studies of these beams. Duane has used EGS4 to do extensive, but geometrically simple simulations, to assist in determining correction factors. Li and Rogers did other EGS4 calculations based on a very crude cylindrical geometry model and partial data on the accelerators[1]. They used the calculated spectra to calculate TPR, $\%dd(10)_{\mathsf{x}}$ and stopping-power ratios using `DDSPR`[2, 3]. A more recent study by Knight included a more sophisticated modelling of the accelerator but it still had several restrictions and its results did not agree particularly well with the measured TPR^{20}_{10} values[4]. In this work we report detail simulations using the BEAM code[5]. We are aware that David Shipley and others at NPL are doing similar calculations (private communication, 1998).

2 The Calculations

2.1 Accelerator model

Figure 1 below shows a schematic of the simulation geometry for the heavily-filtered 19 MV beam. This geometry is based on extensive personal communications with Simon Duane, David Shipley, Alan DuSautoy, Karen Rosser and Rebecca Nutbrown of the NPL. We wish to thank them for their generous help.

The incident electron beam strikes a tungsten target (thickness 5 mm for the 19 MV beam) and the resulting photons pass through 4 cm of aluminum filtration attached to the back of the target. The photons are then collimated by a 2-stage tungsten collimator. There is a tungsten flattening filter (thickness of tungsten = 5 mm for the 19 MV beam) in an aluminum holder between the two collimator stages. 1.14 cm below the lower collimator is a monitor chamber consisting of 4 mm PMMA, 0.5 mm Al, 2 mm air and 0.035 mm kapton. Then, 8 cm below the lower collimator, there is an additional 9 cm of aluminum filtration. The aluminum filtration is, essentially, what differentiates the lightly- and heavily-filtered beams at a given energy. Up to 4 cm of aluminum can be attached to the back of the target, and any additional filtration is placed below the lower collimator. See Table 1 for target, flattening filter and aluminum filtration specs for the different beam energies/filtrations. The tungsten collimator and monitor chamber do not change with beam energy/filtration.

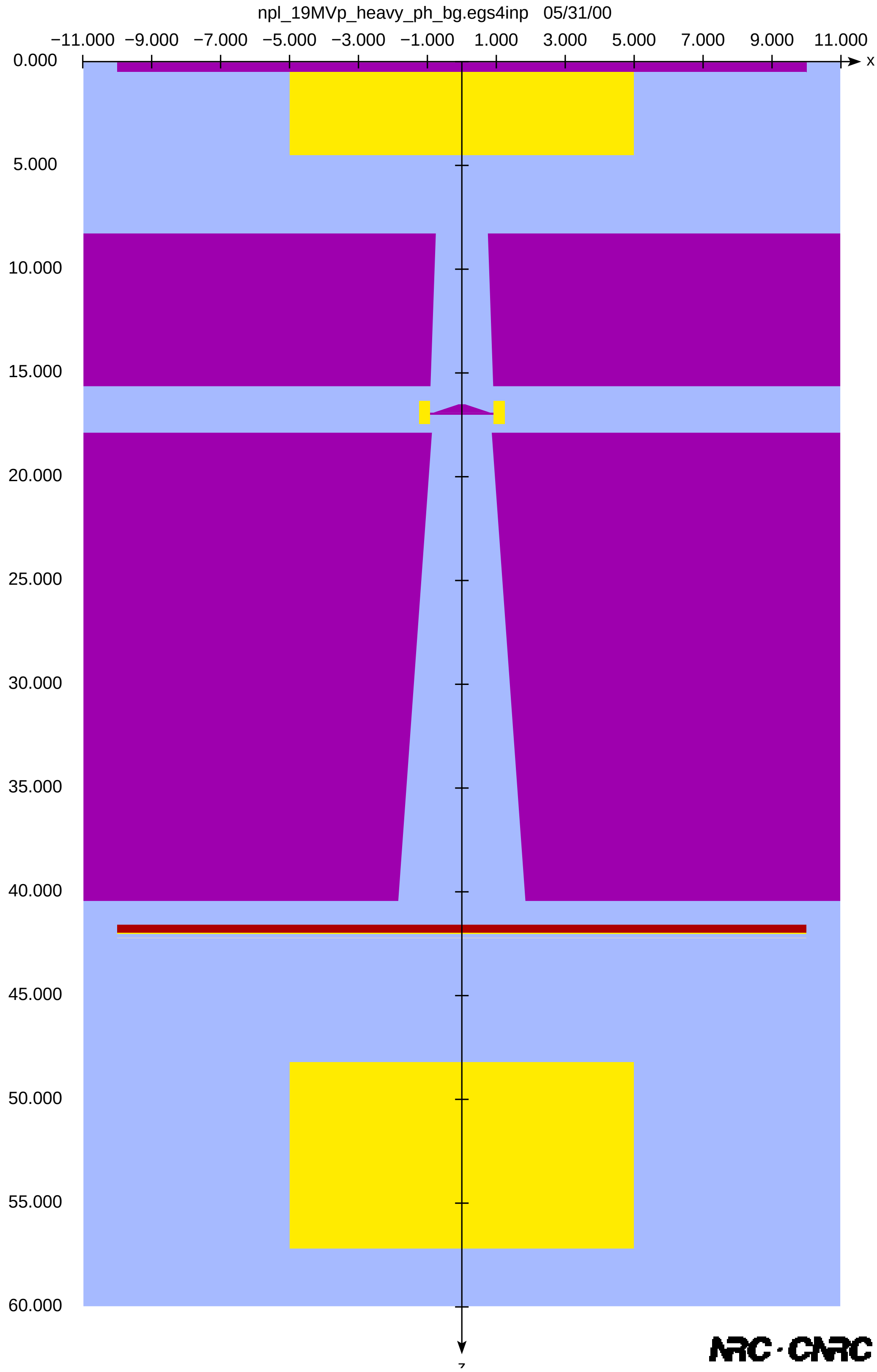

Figure 1: Schematic of the geometry used to simulate the 19 MV heavily-filtered beam. The SSD is 118 cm for this beam.

Table 1: Geometry details for the different beams/filtrations. "L" stands for lightly-filtered and "H" for heavily-filtered beams. For the filtration thickness, the first number is the thickness of Al attached to the back of the target (up to 4 cm) and the second number is the thickness of Al placed below the lower collimator.

energy/ filtration	target thickness (mm W)	flattening filter thickness (mm) + composition	filtration (cm Al)	SSD (cm)
4L	1	3 Cu	0	120
4H	3	3 Cu	4-1	120
6L	3	3 Cu	0	120
6H	3	3 Cu	4-1	120
8L	3	4 Cu	0	120
8H	3	4 Cu	4-6	120
10L	3	5 Cu	0	120
10H	3	5 Cu	4-10	120
12L	3	3 W	0	118
12H	3	3 W	4-9	118
16L	5	4 W	0	118
16H	5	4 W	4-9	118
19L	5	5 W	0	118
19H	5	5 W	4-9	118

Figure 2 below shows the flattening filter for the 19MV beam in detail. Both the composition and the thickness of the flattening filter depend on the beam energy (See Table 1). The aluminum holder is the same for all beams/filtrations. The total thickness of the flattening filter is made up of a cylindrical base (radius 0.925 cm) which is always 0.1 cm thick and a conical section of variable thickness. Regardless of the thickness of the conical section, it has a radius of 0.1 cm at the top and a radius of 0.825 cm at the bottom.

There are some differences between our simulation geometries and those used by Knight[6]. First, our incident electron beam is a solid cone with half-angle 3 degrees, the apex of the cone at the front of the target (Z=0) and spot radius of 0 mm. Knight used an incident parallel beam with radius 0.5 mm. According to Knight himself, the conical model is probably more realistic, however, as we show below (see section 3.3), the difference between the two incident beams has no impact on depth-dose results.

In Knight's simulations, the flattening filter was reversed (ie cone pointing down) and in a slightly different Z position compared to our most recent simulations. Initially, we ran the simulations with the flattening filter having the same orientation and position as Knight's, with the cone pointing down and positioned between $Z = 16.005{+}d$ and $Z = 16.005{+}d{+}t$ cm, where t is the flattening filter thickness and d is the target thickness. More recent information from NPL indicates that (in addition to having the cone pointing up), the flattening filter is positioned between $Z = 17.01 - t$ and $Z = 17.01$ cm. In our latest simulations, we have oriented and positioned the flattening filter according to this recent information, but we have found, that these changes had little effect on the depth-dose results.

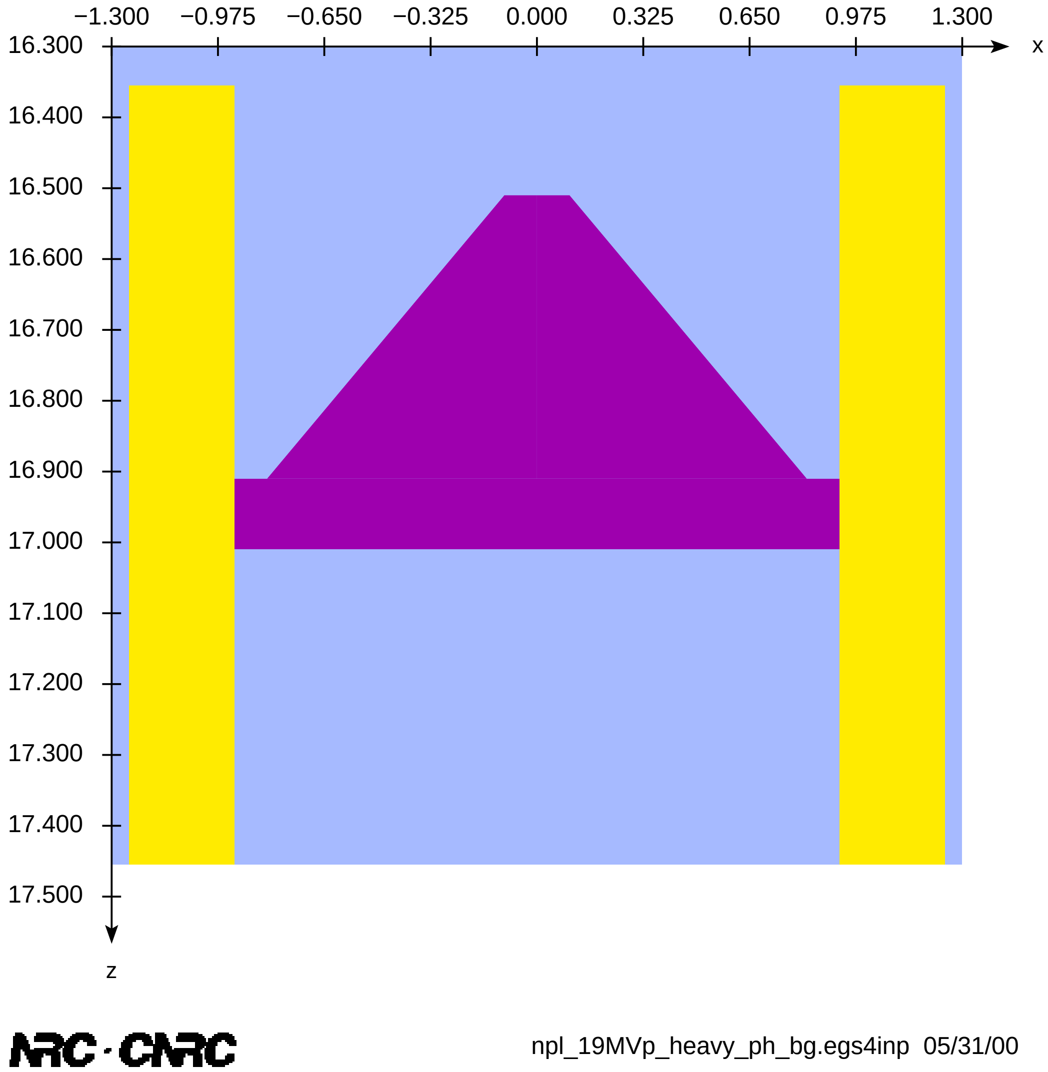

Figure 2: Schematic of the flattening filter used in the 19MV beam simulations.

Knight used slightly different positioning and dimensions for the upper and lower tungsten collimators. His upper collimator started at $Z = 7.0 + d$ cm, where d is the target thickness, and had radius 0.625 cm at the top and 0.96 cm at the bottom, and his lower collimator started at $Z = 16.79 + d$ cm with radius 0.8715 cm at the top and 1.855 cm at the bottom. Again, we used Knight's data initially, but have since changed these to reflect the most recent data from NPL, in which the upper collimator starts at Z=8.28 cm and has radius 0.755 cm at the top and 0.91 cm at the bottom and the lower collimator starts at Z=17.88 cm with radius 0.868 cm at the top and 1.845 cm at the bottom. Comparison of our previous results with current results indicates that these changes in collimator dimension/position have little effect on the depth-dose results.

Knight did not simulate the monitor chamber, and placed additional aluminum filtration only 1cm below the lower tungsten collimator (filtration is 8 cm below the lower collimator in our simulation and according to NPL measurements). Knight also assumed an SSD of 125 cm for all beams, while, based on information from NPL, we use the SSD of 120 cm or 118 cm (See Table 1).

There are also some known differences between our simulation geometry and the actual NPL geometry. First, we have assumed that the flattening filter holder is an aluminum annulus, while the actual structure is more complicated and composed of aluminum, copper, tungsten and lead. We have found that electrons and photons originating in the holder account for no more than 0.1% and 0.002% respectively of electrons/photons reaching the bottom of the accelerator, so the details of the holder are probably not important. We have also not simulated the aluminum holder for the monitor chamber. Again, no particles originating in the monitor chamber reach the bottom of the accelerator, so this omission has no effect.

In terms of simulation parameters, we use a constant ECUT and PCUT of 0.7 MeV and 0.01 MeV respectively, while Knight used a varying ECUT and PCUT depending on beam energy (see Table 7.6 in his thesis). We employ selective bremsstrahlung splitting (max. splitting factor=200, min. splitting factor 20, over a 22x22 cm field at SSD=125 cm) to increase the efficiency of the calculation[7]. Knight, on the other hand, used uniform bremsstrahlung splitting (splitting factor=650) for all simulations. We also use region-by-region range rejection (see Table 2 below for ESAVE values) to increase efficiency. Knight does not appear to have used this[6].

For our depth dose calculations a 30 cm deep CHAMBER phantom was placed starting at the SSD. The dose zones in the phantom all had radius 2 cm. The thickness of the dose zones varied through the depth of the phantom with greater resolution required near the peak of the depth-dose curve to get a good estimate of the maximum dose. Actual dose zone thickness depend on the beam energy/filtration. We also arbitrarily split photons (splitting factor 100) and electrons (splitting factor 40) as they entered the CHAMBER phantom to improve statistics in the depth-dose calculation.

Some simulation parameters used to generate depth-dose curves are shown in Table 2. In this table "L" stands for lightly filtered and "H" stands for heavily filtered beams. Similar to Knight, we assume that the incident electron energy is equal to the nominal beam energy. However, there has been some concern expressed at NPL that the incident energy may be less than the nominal energy by as much as 7%. Knight studied the effects of this possibility in his thesis[6], and we examine the effects of this on our depth-dose calculations below.

Table 2: BEAM simulation parameters for depth-dose calculations using a CHAMBER depth-dose phantom. Simulations were done on 200 MHz Pentium pro CPUs except * which were on 600 MHz Pentium 3 CPUs.

energy/ filtration	ESAVE (MeV)	# histories	CPU time (hrs)
4L	1.0	64x10^6	51.2*
4H	1.0	62.5x10^6	154.0
6L	2.0	34x10^6	173.2
6H	2.0	40x10^6	55.6*
8L	3.0	10x10^6	90.8
8H	3.0	40x10^6	82.6*
10L	3.0	3.5x10^6	48.1
10H	3.0	40x10^6	111.4*
12L	4.0	8x10^6	156.7
12H	4.0	25x10^6	95.5*
16L	5.0	6x10^6	211.3
16H	5.0	22.5x10^6	167.3*
19L	5.0	3.2x10^6	152.9
19H	5.0	10x10^6	102.5*

2.2 Other Calculation Details

Figure 3 shows an example depth-dose curve calculated using BEAM with a CHAMBER depth-dose phantom for the 16 MV lightly-filtered beam.

We calculate $\%dd(10)$ from this curve by taking the total dose at 10 cm depth in the phantom and dividing by the total dose at the peak. $\%dd(10)_{\mathsf{x}}$ can be calculated in the same way using the photon-only depth-dose curve. TPR^{20}_{10} is calculated from the curve using the following equation:

$$TPR^{20}_{10} = \frac{D_{20}}{D_{10}} \times \left(\frac{SSD+20}{SSD+10}\right)^2 \times K_{scatter} \tag{1}$$

where D_{20} is the dose at 20 cm depth, D_{10} is the dose at 10 cm depth and $K_{scatter}$ is a correction factor determined by Yang et al[8]. A plot of the $K_{scatter}$ correction factor as a function of TPR^{20}_{10} determined from D_{20}/D_{10} is shown in Figure 4 below. $K_{scatter}$ varies from 3.5% at ^{60}Co to about 1% for a TPR^{20}_{10} of 0.8 but is only known to about 0.3% because the size of the correction for a given TPR^{20}_{10} value can vary depending on other details of the beam quality[8]. These values are consistent with the experimental data of Followill et al[9] which has an even greater statistical spread.

Using $\%dd(10)$ and $\%dd(10)_{\mathsf{x}}$ from the BEAM depth-dose curve, we can obtain a correc-

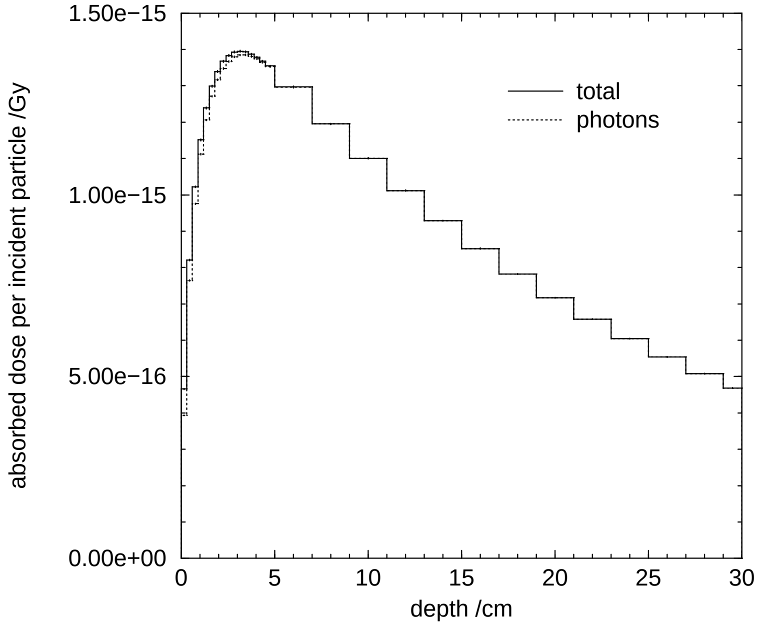

Figure 3: Depth-dose curves for the 16 MV lightly-filtered beam. BEAM allows us to plot both the total depth-dose curve and the contribution due to photons only at an SSD of 118 cm.

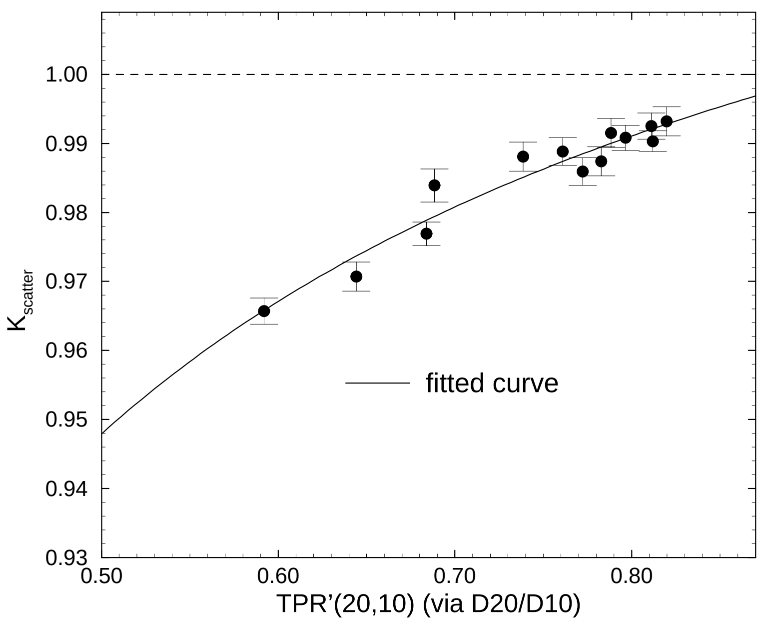

Figure 4: $K_{scatter}$ vs TPR_{10}^{20} determined from D_{20}/D_{10}. In this study, the fitted curve was used to obtain $K_{scatter}$ values.

tion for electron contamination, ϵ, where:

$$\epsilon = \left[\frac{\%dd(10)_{\mathsf{x}}}{\%dd(10)}\right]_{BEAM} \tag{2}$$

The value of ϵ can then be used to convert NPL measured values of $\%dd(10)$ to an estimate of $\%dd(10)_{\mathsf{x}}$ at the NPL SSD (see Tables 6 and 8). However, we still require an additive factor to convert the estimated $\%dd(10)_{\mathsf{x}}$ at the SSD of the NPL beam to $\%dd(10)_{\mathsf{x}}$ at an SSD of 100 cm. In order to do this, we use the BEAM calculated photon spectrum from the NPL simulations as input to the program `DDSPR`[2]. `DDSPR` will then calculate $\%dd(10)_{\mathsf{x}}$ for any SSD for a parallel beam. We then convert from a parallel beam to a point source by using a $1/\mathrm{r}^2$ correction factor as well as a factor determined by Yang, et al[8], K_{PS}, which depends on the value of $\%dd(10)_{\mathsf{x}}$. Thus, the additive factor, Δ, is given by:

$$\Delta = K_{PS} \times [\%dd(10)_{\mathsf{x}}(SSD = 100cm)]_{DDSPR} - K_{PS} \times [\%dd(10)_{\mathsf{x}}(NPL\ SSD)]_{DDSPR} \tag{3}$$

Note that this method assumes that the photon spectrum at SSD=100 cm is the same as at the NPL SSDs. We also approximate that the value of K_{PS}, determined by Yang, et al at SSD=100 cm, is the same for a given value of $\%dd(10)_{\mathsf{x}}$ at the NPL SSD. K_{PS} as a function of $\%dd(10)$ determined for a parallel beam is shown in Figure 5 below.

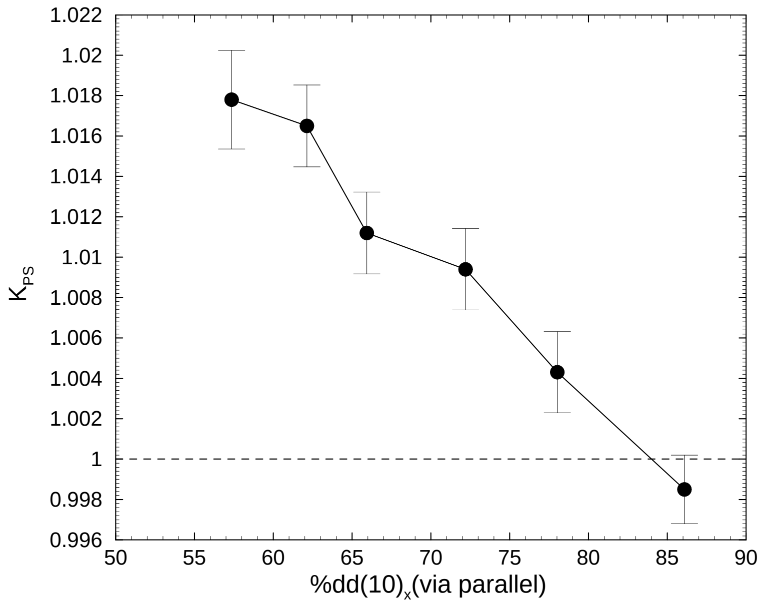

Figure 5: K_{PS} vs $\%dd(10)$ for a parallel beam. K_{PS} values in this study were taken from a straight line drawn through the points on this curve.

There is a question as to whether the photon spectrum on the central axis or over the entire field should be used as input to `DDSPR`. We attempt to resolve this by using both the central axis spectrum (r=0-2.25 cm) and the spectrum over the entire field (r=0-5.8 cm) as input to `DDSPR` for all beam energies/filtrations and determining which spectrum gives $\%dd(10)_{\mathsf{x}}$ at the NPL SSD closest to the the $\%dd(10)_{\mathsf{x}}$ calculated from the BEAM depth-dose curve.

Once ϵ and Δ have been calculated, then an estimate of measured $\%dd(10)_x$ can be calculated from:

$$[\%dd(10)_x(SSD = 100cm)] = \epsilon\,[\%dd(10)(NPL\ SSD)]_{meas.} + \Delta \quad (4)$$

3 Dependence on model details

3.1 Effect of Beam Spot Radius

The simulations described above all assume that the radius of the incident conical electron beam is zero where it is incident on the target (ie at Z=0). It is known, however, that the incident beam has a finite radius where it strikes the target. This radius is reported to vary anywhere from 1 mm to 1 cm. To obtain an understanding of how this spot radius affects the beam, most specifically, the value of $\%dd(10)_x$, we have simulated various incident beam spot radii for the 4MVL and 19MVL accelerators.

Figure 6 below shows the energy fluence distributions for the 19MVL beam at SSD=118 cm for beam spot radii of 0 cm and 1 cm.

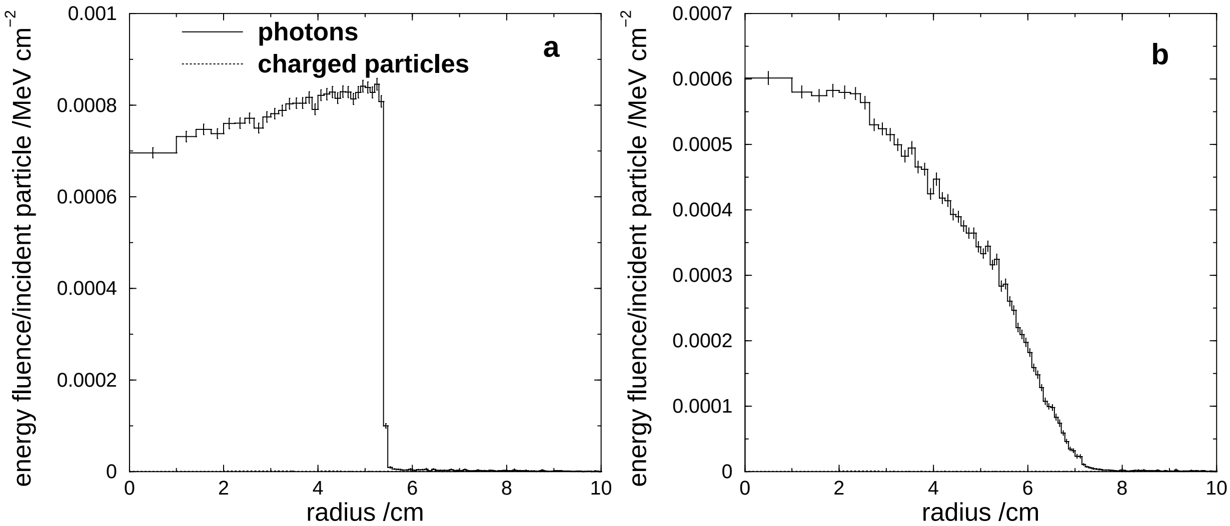

Figure 6: Energy fluence profiles at SSD=118 cm for the 19MVL accelerator with a conical incident beam having a spot radius of (a) 0 cm and (b) 1 cm. The energy fluence of photons and charged particles is shown in each case.

The beam spot radius has a definite effect on the energy fluence profile. With a beam spot radius of 0 cm, the energy fluence actually increases with increasing radius before dropping off quickly at the edge of the field. The spot radius of 1 cm causes the energy fluence to drop off quickly with increasing radius, resulting in a narrower effective field radius. In addition the increased spot radius decreases the efficiency of the calculation. This is seen in the lower overall energy fluence/incident particle in Figure 6(b).

Figure 7 below shows normalized photon energy fluence spectra at SSD=118 cm for the 19MVL beam with an incident spot radius of 0 and 1 cm. Spectra are shown on the central axis (r=0-2.25 cm) and over the entire field (r=0-5.8 cm).

From the Figure 7, it is evident that the spot size has no major effect on the shape of spectrum either on the central axis or over the entire field.

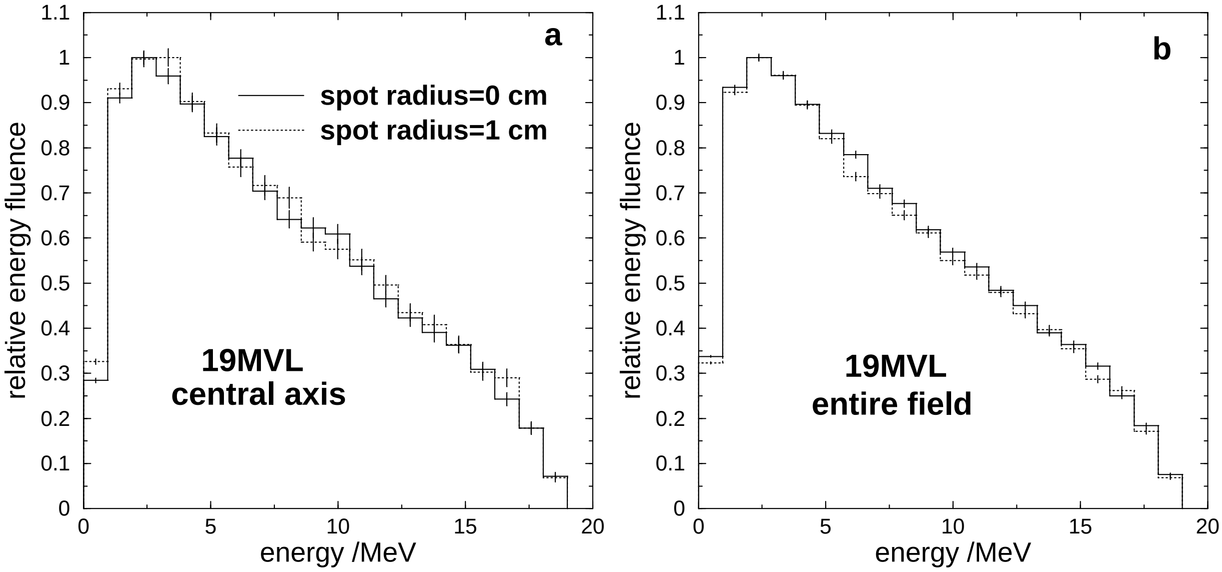

Figure 7: Photon energy fluence spectra at SSD=118 cm for the 19MVL beam with an incident beam spot radius of 0 cm and 1 cm. Spectra are shown (a) for the central axis (r=0-2.25 cm) and (b) for the entire field (r=0-5.8 cm). Spectra have been normalized to their peak values.

Table 3 below shows values of $\%dd(10)_{\mathsf{x}}$ and TPR^{20}_{10} calculated for various spot radii in the 4MVL and 19MVL beams. For each spot radius, $\%dd(10)_{\mathsf{x}}$ and TPR^{20}_{10} were determined using the central axis photon spectrum and the spectrum over the entire field as input to the program `DDSPR`. `DDSPR` then calculates the value of $\%dd(10)_{\mathsf{x}}$, automatically applying a $1/\mathrm{r}^2$ factor to convert from parallel beam to point source, on top of which we apply the parallel-point source correction factor, K_{PS} (see Equation 3 and [8]). The values of $\%dd(10)_{\mathsf{x}}$ and TPR^{20}_{10} calculated using the CHAMBER depth-dose phantom in BEAM are also shown for some cases.

From these results, we conclude that spot size has little effect on the values of $\%dd(10)_{\mathsf{x}}$ and TPR^{20}_{10} calculated using `DDSPR` because the photon spectra on the central axis and over the entire field do not change appreciably. The BEAM results, on the other hand, reflect the the change in photon energy fluence shown in Figure 6, with the narrower effective field at a spot radius of 1 cm causing significant decreases in $\%dd(10)_{\mathsf{x}}$ and TPR^{20}_{10} in both the 4MVL and 19MVL cases. These decreased values of $\%dd(10)_{\mathsf{x}}$ (and $\%dd(10)$) and TPR^{20}_{10} do not agree as well with measurment as those calculated using BEAM with a 0 mm spot radius (see Figure 8).

Unless otherwise noted, the calculations in the rest of the report are done for an incident conical beam with a spot size of 0 mm.

Table 3: Calculated $\%dd(10)_x$ (including K_{PS} correction, see Equation 3) and TPR^{20}_{10} for various spot radii in the 4MVL and 19MVL beams. Values were determined by using the BEAM-calculated photon spectra both on the central axis ("CA"–r=0-2.25 cm) and over the entire field ("EF"–r=0-5.8 cm) as input to DDSPR. Also shown for comparison are some values calculated using the full BEAM simulation.

energy	spot radius	$\%dd(10)_x$ – DDSPR CA	$\%dd(10)_x$ – DDSPR EF	TPR^{20}_{10} – DDSPR CA	TPR^{20}_{10} – DDSPR EF	$\%dd(10)_x$ BEAM	TPR^{20}_{10} BEAM
4L	0cm	62.1	61.9	0.586	0.585	61.4(2)	0.582(2)
4L	1cm	62.0	62.0	0.586	0.585	60.3(1)	0.576(1)
19L	0cm	82.1	82.0	0.765	0.763	81.9(2)	0.761(3)
19L	0.2cm	82.2	82.0	0.765	0.763	NA	NA
19L	0.5cm	82.2	82.1	0.764	0.763	NA	NA
19L	1cm	82.1	82.0	0.763	0.763	80.8(2)	0.752(2)

3.2 Effect of 7% Decrease in Incident Electron Energy

We performed the studies in this section and Section 3.3 below before we had complete information from NPL about the geometry of their accelerator. In particular, they were performed with the flattening filter reversed (cone down) and in the incorrect Z position as in Knight's simulations (see Section 2.1 above). Also we used Knight's dimensions/positions for the upper and lower tungsten collimators instead of the more recent NPL-measured values. However, since we have found that these details have no significant effect on the depth-dose results, the conclusions from this section are still valid.

There have been some questions raised at NPL about the possibility that the actual electron energy on target is 7% lower than the nominal beam energies. This led us to simulate the 4L and 19L beams with a 7% drop in incident energy to see the effect on the depth-dose results.

The results with a 7% drop in incident energy compared to the nominal energy are shown in table 4 below.

Table 4: Values of $\%dd(10)$, $\%dd(10)_x$ and TPR^{20}_{10} calculated from BEAM depth dose curves for the 4L and 19L beams with incident energy equal to the nominal energy and with incident energy 7% less than nominal. Measured values are also shown for $\%dd(10)$ and TPR^{20}_{10}.

beam	%dd(10)			$\%dd(10)_x$		TPR^{20}_{10}		
	less 7%	nominal	meas.	less 7%	nominal	less 7%	nominal	meas.
4L	60.9(2)	61.6(1)	63.0	61.0(2)	61.8(2)	0.572(2)	0.584(2)	0.587
19L	80.2(2)	81.3(2)	80.6	81.0(2)	81.9(2)	0.757(2)	0.761(3)	0.764

For both beams, the effect of a 7% drop in incident energy is to decrease $\%dd(10)$ and $\%dd(10)_x$ by 1%. Behaviour of the TPR^{20}_{10} is different, though. In the 4L case, it dropped by 2%, while in the 19L case it dropped by only 0.5%. This observation of the effect of the 7% drop on TPR^{20}_{10} decreasing with increasing energy is consistent with Figure 10.4 in Knight's thesis.

In almost all cases, the 7% decrease in incident energy makes the agreement between the calculations and measurements worse, suggesting that the nominal energies are probably correct. Detailed conclusions based on these results are saved until section 7, after the general results have been presented.

3.3 Effect of Conical vs Parallel Incident Beam

As stated in section 2.1 above, we used a conical incident electron beam (cone angle of 3 degrees with the apex of the cone at the front of the target), while Knight's simulations used a parallel incident beam (radius=0.05 cm)[6]. Although the conical beam is thought to be more realistic, we performed several simulations with the parallel incident beam for comparison and to see what effect the the parallel incident beam might have had on Knight's results.

Table 5 below summarizes the results of the BEAM depth-dose calculations done for the 4L and 19L beams with both conical and parallel (radius=0.05 cm) incident beams.

Table 5: Values of $\%dd(10)$, $\%dd(10)_{\mathsf{x}}$ and TPR^{20}_{10} calculated from BEAM depth dose curves for the 4L and 19L beams with conical incident electron beams and parallel incident electron beams (radius=0.05 cm).

beam	%dd(10)		$\%dd(10)_{\mathsf{x}}$		TPR^{20}_{10}	
	$\|\|$	cone	$\|\|$	cone	$\|\|$	cone
4L	61.5(2)	61.6(1)	61.6(2)	61.8(2)	0.584(2)	0.584(2)
19L	81.4(2)	81.3(2)	82.1(2)	81.9(2)	0.764(2)	0.761(3)

From the table, it is evident that there is no significant difference between the depth-dose results obtained using a conical incident beam and those obtained with a parallel incident beam similar to Knight's.

4 Depth-dose and TPR calculations using BEAM

Table 6 below shows the results of the BEAM depth-dose calculations using the simulation parameters described in section 2.1.

Table 6: Values of $\%dd(10)$, $\%dd(10)_x$ and TPR_{10}^{20} calculated from the BEAM depth-dose curves. Also shown are recent NPL-measured values of $\%dd(10)$ and TPR_{10}^{20} ("meas."), the standard values of TPR_{10}^{20} that NPL gives out ("NPL std."), and Richard Knight's calculated values of TPR_{10}^{20}[6].

energy/ filtration	%dd(10)		$\%dd(10)_x$	D_{20}/D_{10}	TPR_{10}^{20}			
	calc.	meas.			calc.	meas.	NPL std.	Knight
Co-60								
4L	61.4(2)	63.0	61.4(2)	51.8(1)	0.582(2)	0.587	0.584	0.595
4H	64.0(3)	65.1	64.1(3)	54.5(2)	0.616(3)	0.621	0.621	0.617
6L	66.7(2)	67.1	66.9(2)	57.0(2)	0.646(2)	0.647	0.646	0.649
6H	68.1(2)	68.4	68.3(2)	58.4(2)	0.663(2)	0.666	0.670	0.665
8L	69.9(2)	70.7	70.2(2)	59.7(2)	0.679(2)	0.678	0.679	0.681
8H	72.7(2)	72.7	73.0(2)	62.5(1)	0.714(2)	0.714	0.717	0.716
10L	72.6(2)	72.6	72.9(2)	61.6(1)	0.702(2)	0.703	0.704	0.708
10H	75.9(2)	75.9	76.3(2)	65.1(2)	0.744(2)	0.746	0.746	0.748
12L	74.9(2)	74.3	75.3(1)	63.12(9)	0.722(1)	0.719	0.723	0.727
12H	77.6(1)	77.9	78.1(1)	65.94(9)	0.756(1)	0.758	0.758	0.762
16L	78.9(2)	78.0	79.4(1)	65.10(9)	0.747(1)	0.745	0.750	0.752
16H	81.2(1)	81.3	81.9(1)	67.6(1)	0.777(1)	0.780	0.779	0.780
19L	81.3(2)	80.6	81.9(2)	66.3(2)	0.761(2)	0.764	0.763	0.765
19H	83.2(2)	82.9	84.2(2)	68.4(2)	0.786(2)	0.791	0.790	0.791

Figure 8 shows the ratios of calculated and recently-measured values of $\%dd(10)$ and TPR_{10}^{20} as a function of beam energy. The ratios of calculated and NPL standard TPR_{10}^{20} values are also shown. Agreement between the calculated and the recently measured and standard TPRs is better than that between the calculated and the measured $\%dd(10)$. The maximum difference between the calculated and recently measured TPRs is 0.9% and is 1.0% between the calculated and standard set of NPL TPR values. The rms deviations are 0.5% and 0.4% respectively for the same comparisons. For the measured $\%dd(10)$ values the maximum deviation of the calculations is 2.5% and the rms deviation is 1.0%, although for the heavily filtered beams of 6MV and above the agreement is better than 0.5%.

To summarize, the agreement with the measured values of $\%dd(10)$ and TPR_{10}^{20} for the heavily filtered beams used for the NPL calibration services is excellent except for the 4MV beam. The agreement for the lightly filtered beams is also quite good, again with the exception of the 4MV beam.

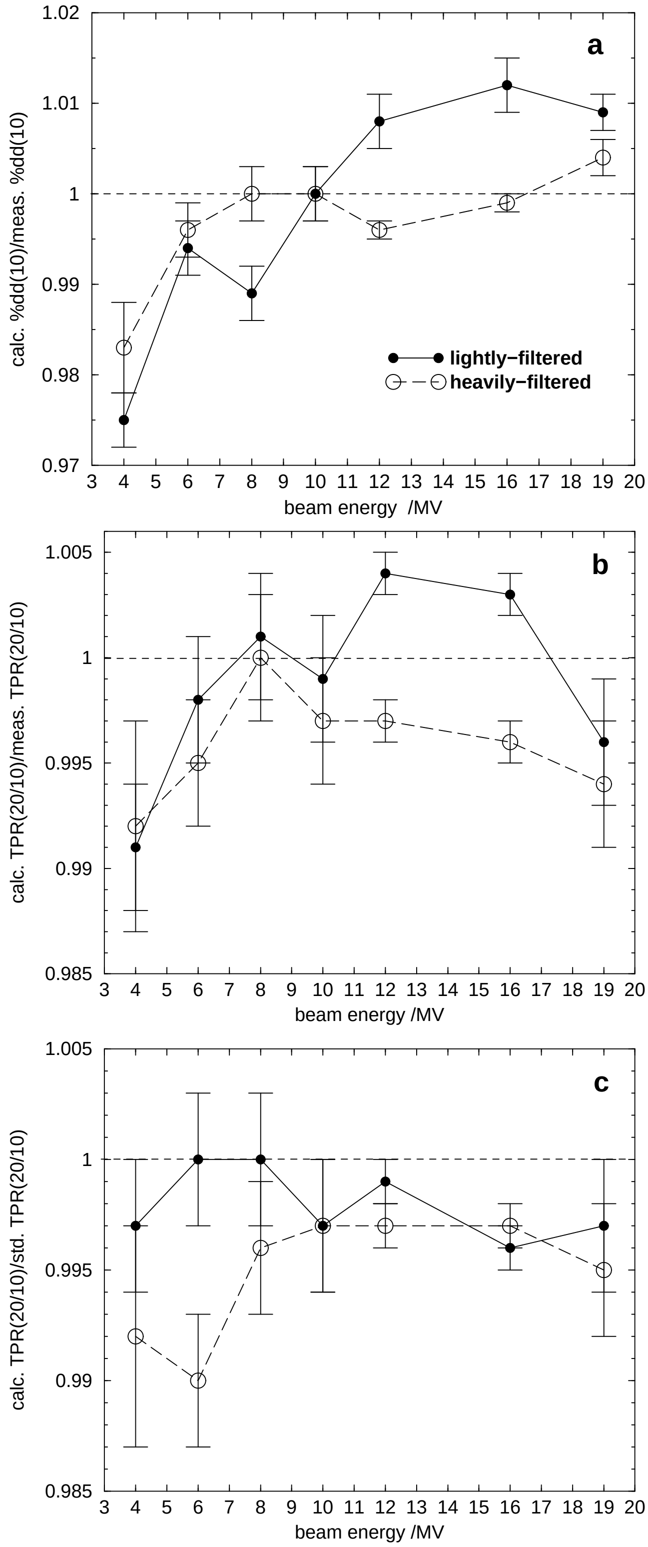

Figure 8: Fractional difference between (a) $\%dd(10)$ calculated from the BEAM depth-dose curves and recently measured at NPL, (b) TPR^{20}_{10} calculated from BEAM and recently measured at NPL and (c) TPR^{20}_{10} from BEAM and the standard NPL values as functions of beam energy. Note that (b) and (c) have a much smaller vertical scale than (a).

4 DEPTH-DOSE AND TPR CALCULATIONS USING BEAM

5 Depth-dose and TPR calculations using DDSPR

We used photon spectra generated by BEAM simulations as input to the program `DDSPR`. `DDSPR` calculates the value of $\%dd(10)_{\mathsf{x}}$ for any SSD and field size assuming a parallel incident beam. `DDSPR` then automatically applies a $1/\mathrm{r}^2$ factor to convert from a parallel beam to a point source, and we apply the correction factor, K_{PS} determined by Yang, et al[8]. For each beam, the photon spectra were generated using a geometry identical to that used in the BEAM depth-dose calculations with the exception that the CHAMBER depth-dose phantom was effectively turned off by setting ECUT=PCUT=25 MeV. In addition, photon interaction forcing and photon/electron splitting inside the phantom were turned off. Phase space files were then generated in the plane at the top of the phantom (ie at the SSD). For each energy/filtration, enough histories were run to generate 200,000 particles in the phase space file. Note that these runs were much shorter than those required for the depth-dose calculations. Spectra were then generated from the phase spacefile using the program `beamdp`. We generated spectra on the central axis (r=0-2.25 cm) and over the entire field (r=0-5.8 cm) and used both as input to `DDSPR`.

The photon spectra for the 19L and 19H beams over the central axis and over the entire field are shown in figure 9 below.

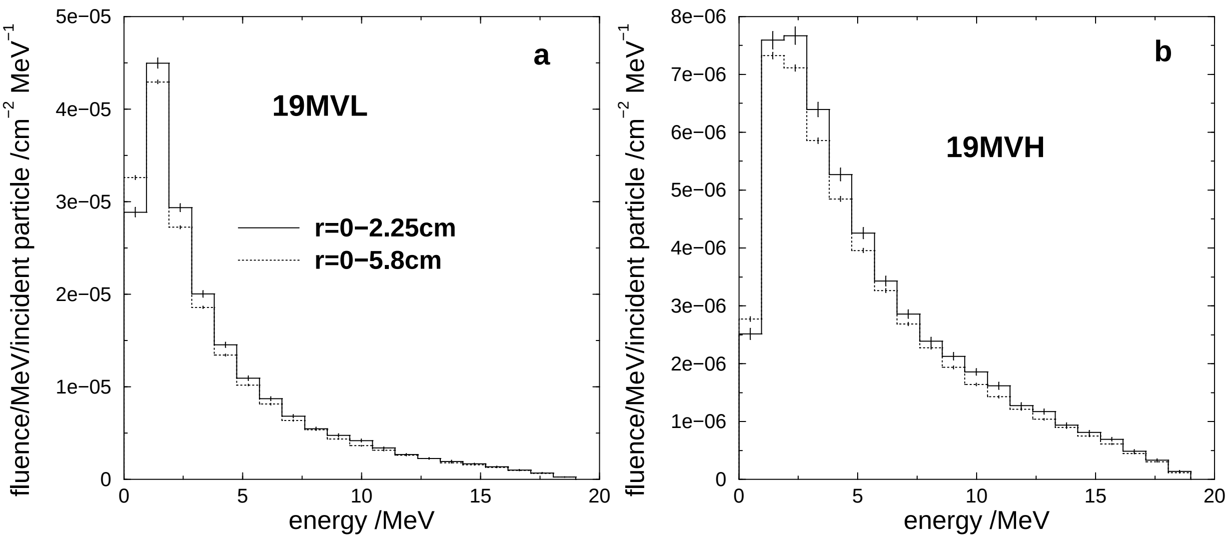

Figure 9: Photon spectra calculated using BEAM for the 19 MV beam (a) lightly-filtered and (b) heavily-filtered. Spectra are shown for both the central axis (r=0-2.25 cm) and over the entire field (r=0-5.8 cm).

Note the hardening effect of the additional Al filtration in the 19H case. There are some significant differences between the central-axis spectra and the spectra over the entire field, especially at lower energies, that have an effect on $\%dd(10)_{\mathsf{x}}$ and TPR^{20}_{10} calculated by `DDSPR`.

Table 7 below summarizes the results of the `DDSPR` depth-dose calculations, both at the NPL SSD's (120 cm or 118 cm) and at SSD=100 cm. At both SSD's, results are shown for both the central axis spectrum (CA) and the spectrum over the entire field (EF). The

BEAM depth-dose results at the NPL SSD's are also shown for reference.

Table 7: $\%dd(10)_x$ and TPR^{20}_{10} calculated using photon spectra generated by BEAM as input to DDSPR. $\%dd(10)_x$ results require conversion from parallel beam to point source results using a $1/r^2$ factor (done automatically by DDSPR) and the correction factor, K_{PS}[8]. Results are shown using both the central axis ("CA"–r=0-2.25 cm) photon spectra and the photon spectra over the entire field ("EF"–r=0-5.8 cm) at the NPL SSD's and SSD=100 cm. In all cases, a field radius of 5.6cm was used in the DDSPR calculations. Results from the full BEAM calculation are shown for comparison. TPR^{20}_{10} was calculated from the BEAM results using Equation 1.

beam	at NPL SSD						at SSD=100 cm	
	$\%dd(10)_x$			TPR^{20}_{10}			$\%dd(10)_x$	
	CA	EF	BEAM	CA	EF	BEAM	CA	EF
4L	62.1	61.9	61.4(2)	0.586	0.585	0.582(2)	60.5	60.3
4H	64.7	64.6	64.1(3)	0.618	0.617	0.616(3)	63.1	63.0
6L	67.6	67.5	66.9(2)	0.648	0.647	0.646(2)	65.9	65.8
6H	69.1	68.9	68.3(2)	0.667	0.665	0.663(2)	67.4	67.2
8L	70.8	70.8	70.2(2)	0.680	0.679	0.679(2)	69.2	69.2
8H	73.5	73.5	73.0(2)	0.713	0.713	0.714(2)	71.7	71.7
10L	73.8	73.5	72.9(2)	0.706	0.703	0.702(2)	72.2	72.0
10H	76.9	76.8	76.3(2)	0.746	0.744	0.744(2)	75.3	75.2
12L	76.1	75.9	75.3(1)	0.727	0.724	0.722(1)	74.7	74.4
12H	78.6	78.5	78.1(1)	0.759	0.758	0.756(2)	77.1	77.0
16L	79.7	79.6	79.4(1)	0.751	0.749	0.747(1)	78.3	78.2
16H	82.1	82.1	81.9(1)	0.779	0.780	0.777(1)	80.7	80.8
19L	82.1	82.0	81.9(2)	0.765	0.763	0.761(2)	80.8	80.7
19H	84.4	84.3	84.2(2)	0.791	0.790	0.786(2)	83.2	83.2

Figure 10 below shows the fractional difference between DDSPR calculated values of $\%dd(10)_x$ and TPR^{20}_{10} at the NPL SSD's and their corresponding BEAM-calculated values.

Figure 10 emphasizes that the DDSPR results using the central axis (CA) photon spectrum do not differ significantly from those using the entire field (EF) photon spectrum. Also, the DDSPR/BEAM ratios for lightly-filtered beams do not differ significantly from those for heavily-filtered beams at the same energy. The most obvious trend in Figure 10 is the better agreement between DDSPR- and BEAM-calculated values of $\%dd(10)_x$ at higher beam energies.

Figure 11 below shows the values of Δ [$\equiv \%dd(10)_x$(SSD=100 cm)$-\%dd(10)_x$(NPL SSD), see Equation 3], as a function of beam energy for (a) the lightly-filtered beams and (b) the heavily-filtered beams.

Figure 11 shows that the differences calculated using the central axis photon spectra and those calculated using the spectra over the entire field are very close. Another trend of note is that the difference between $\%dd(10)_x$(SSD=100 cm) and $\%dd(10)_x$(NPL SSD) decreases with increasing beam energy.

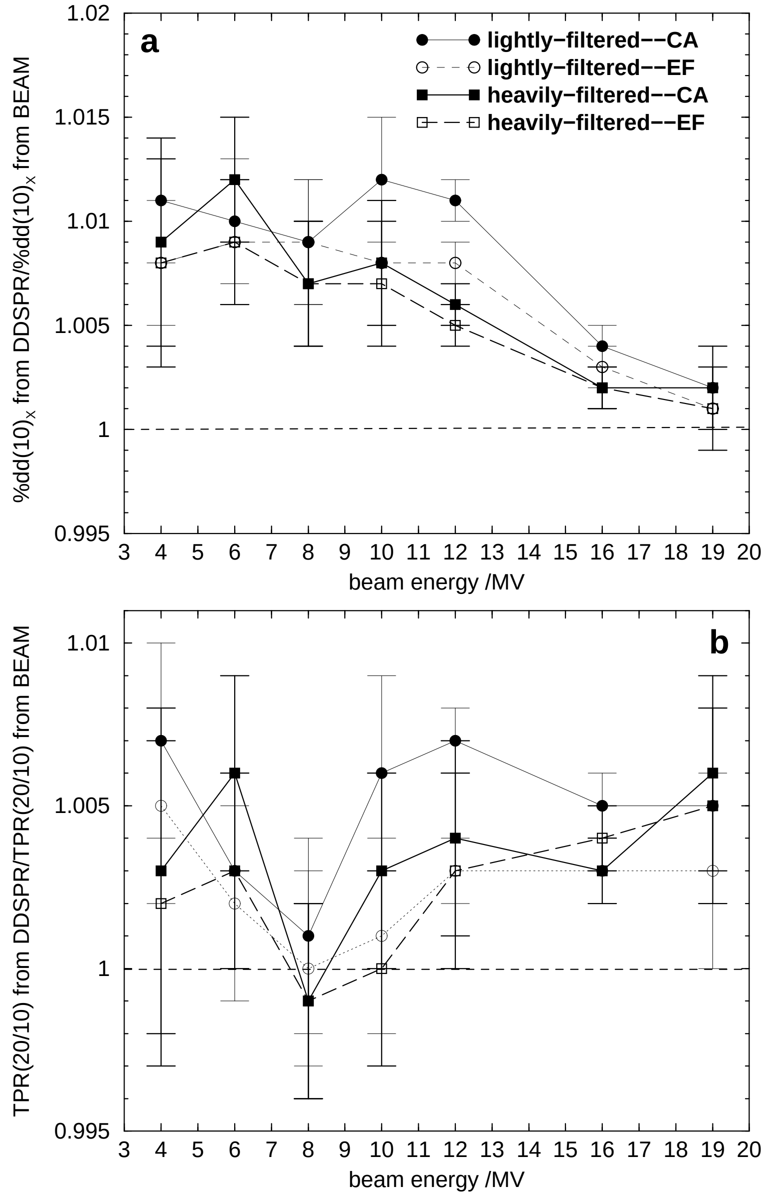

Figure 10: Ratio of DDSPR- to BEAM-calculated values of (a) $\%dd(10)_x$ and (b) TPR_{10}^{20} at the NPL SSD's as a function of beam energy. The thin lines are the results for the lightly-filtered beams and the thicker lines are for the heavily-filtered beams. Fractional differences are shown for when the the central axis photon spectrum (CA) or the photon spectrum over the entire field (EF) is used as input to DDSPR.

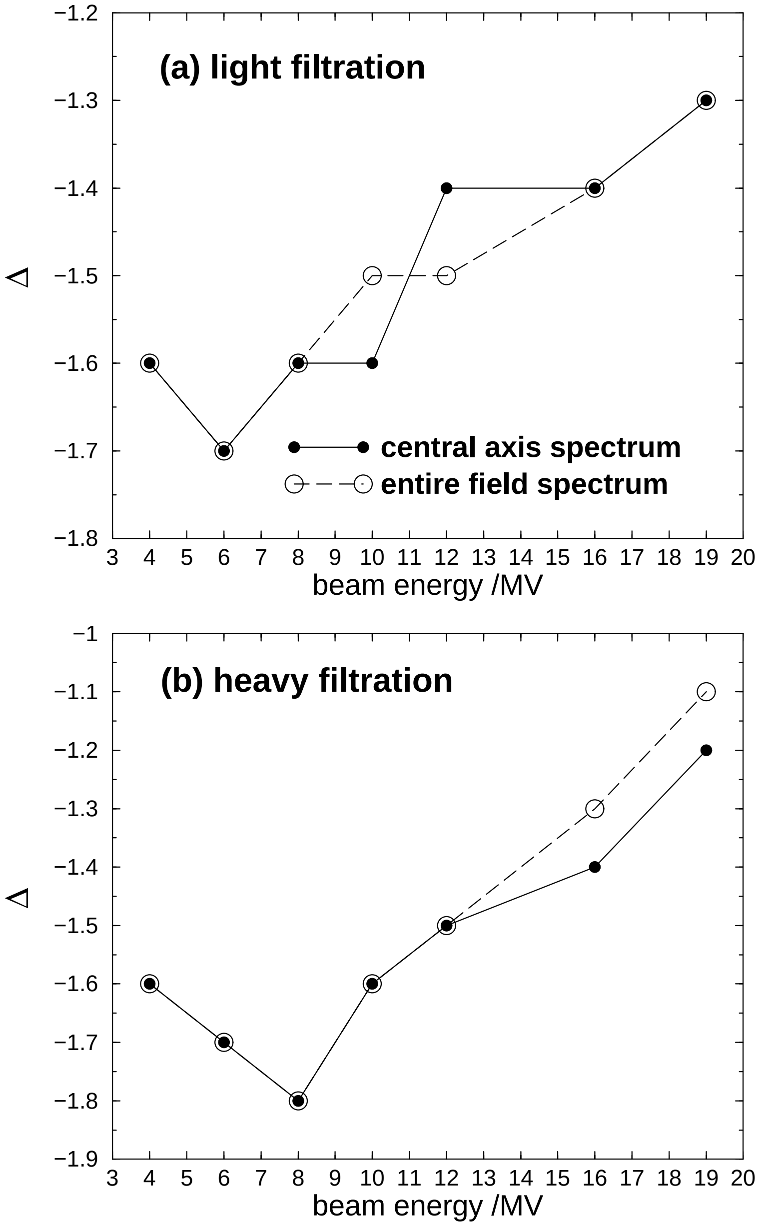

Figure 11: The quantity Δ [$\equiv \%dd(10)_x$(SSD=100 cm)$-\%dd(10)_x$(NPL SSD)] as a function of beam energy for (a) the lightly-filtered and (b) the heavily-filtered beams. Differences are shown using both the central axis photon spectrum and the spectrum over the entire field as input to DDSPR.

5 DEPTH-DOSE AND TPR CALCULATIONS USING DDSPR

6 $\mathbf{k}_Q$ vs $\%dd(10)_{\mathsf{x}}$ and TPR_{10}^{20}

Table 8 presents the measured values of k_Q, TPR_{10}^{20} and $\%dd(10)$ at the NPL SSD along with the conversion factors ϵ, calculated using equation (2) with the data in Table 6, and Δ, calculated using equation (3) (using the photon spectrum over the entire field as input to `DDSPR` and shown in Figure 11), and the estimate of measured $\%dd(10)_{\mathsf{x}}$ at SSD=100 cm calculated using equation (4).

Table 8: Measured k_Q, TPR_{10}^{20} (recently measured and NPL standard values) and $\%dd(10)$ at the NPL SSD, the conversion factors ϵ and Δ and the estimate of measured $\%dd(10)_{\mathsf{x}}$ at SSD=100 cm for each beam.

beam	k_Q	TPR_{10}^{20} meas.	TPR_{10}^{20} std.	$\%dd(10)$ at NPL SSD	ϵ	Δ	$\%dd(10)_{\mathsf{x}}$ at SSD=100 cm
4L	0.99417	0.587	0.584	63.0	1.000(5)	-1.6	61.4(3)
4H	0.99867	0.621	0.621	65.1	1.002(7)	-1.6	63.6(4)
6L	0.99378	0.647	0.646	67.1	1.003(4)	-1.7	65.6(3)
6H	0.99416	0.666	0.670	68.4	1.003(4)	-1.7	66.9(3)
8L	0.9905	0.678	0.679	70.7	1.004(4)	-1.6	69.4(3)
8H	0.98849	0.714	0.717	72.7	1.004(4)	-1.8	71.2(3)
10L	0.98794	0.703	0.704	72.6	1.004(4)	-1.5	71.4(3)
10H	0.98152	0.746	0.746	75.9	1.005(4)	-1.6	74.7(3)
12L	0.98417	0.719	0.723	74.3	1.005(3)	-1.5	73.2(2)
12H	0.9781	0.758	0.758	77.9	1.006(2)	-1.5	76.9(2)
16L	0.97833	0.745	0.750	78.0	1.006(3)	-1.4	77.1(2)
16H	0.97176	0.780	0.779	81.3	1.009(2)	-1.3	80.7(2)
19L	0.97601	0.764	0.763	80.6	1.007(3)	-1.3	79.9(2)
19H	0.96702	0.791	0.790	82.9	1.012(3)	-1.1	82.8(2)

k_Q is plotted as a function of TPR_{10}^{20} (both recently-measured and NPL standard values) and the estimate of $\%dd(10)_{\mathsf{x}}$(SSD=100 cm) in Figure 12.

From Figure 12 it is evident that, at least in terms of consistency between lightly-filtered and heavily-filtered measurements, k_Q is better specified by $\%dd(10)_{\mathsf{x}}$ than by TPR_{10}^{20}. There is also evidence from all three graphs that there may be problems with the 4L and 19L measurements since both create anomalies in the curves for the lightly-filtered beams.

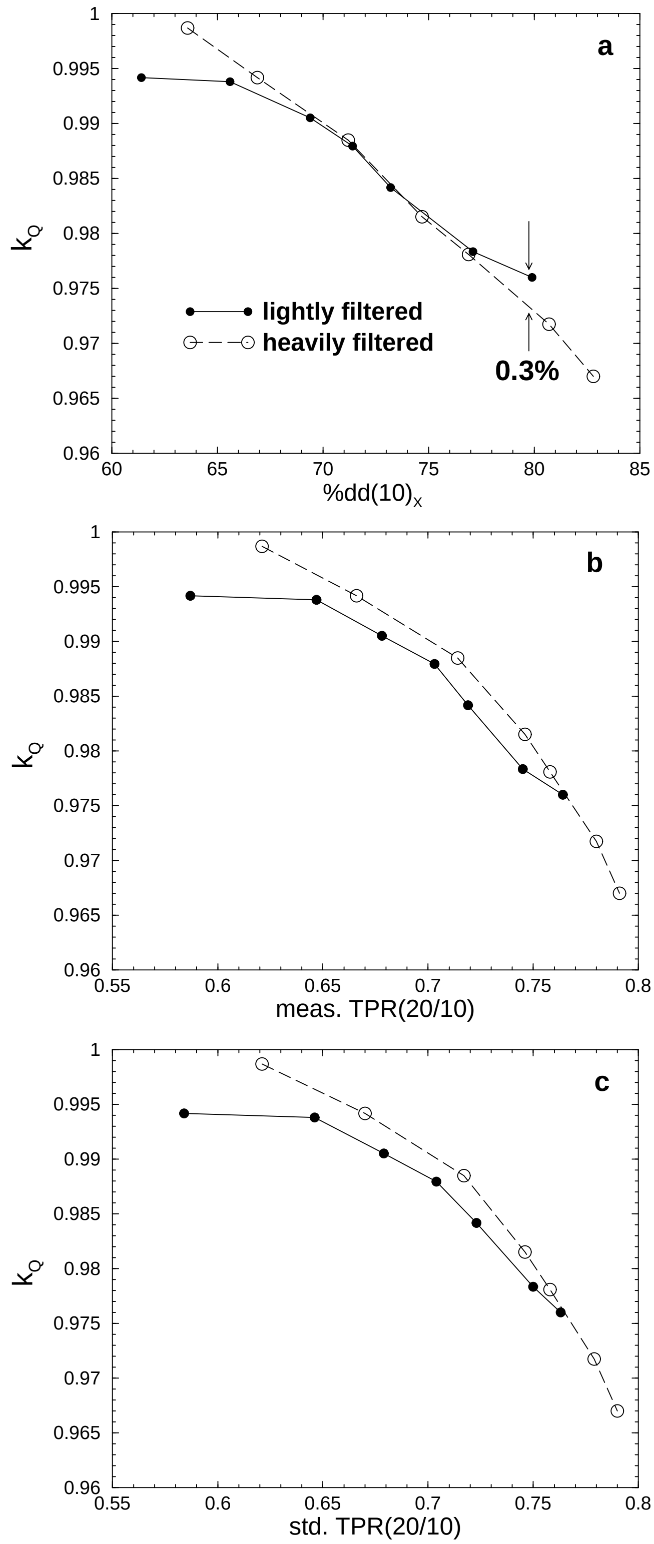

Figure 12: Measured k_Q values vs (a) the estimate of measured $\%dd(10)_x$ at SSD=100 cm, (b) recently-measured TPR^{20}_{10} and (c) NPL standard TPR^{20}_{10}. Results from the lightly-filtered and heavily-filtered beams are plotted as separate curves in each graph.

6 K_Q VS $\%DD(10)_x$ AND TPR^{20}_{10}

7 Summary and Conclusions

Monte Carlo calculations have been shown to calculate $\%dd(10)$ and TPR^{20}_{10} values which are in good agreement with the standard photon beams used at NPL, with the possible exception of the 4 MV beam where both the calculated $\%dd(10)$ and TPR^{20}_{10} values appear to be somewhat low compared to measurement(see fig.8).

We can conclude that the simulation models are reasonably accurate. We have presented methods whereby we extract the beam quality specifier $\%dd(10)_{\mathsf{x}}$ by calculating corrections to the measured values of $\%dd(10)$. It is impossible with the present NPL setup to measure $\%dd(10)_{\mathsf{x}}$ because the setup does not allow going to a $10{\times}10$ cm^2 beam at SSD = 100 cm.

Based on the results of calculations with the incident energy reduced by 7% and considering the comparison of measured vs calculated $\%dd(10)_{\mathsf{x}}$ and TPR^{20}_{10} in fig. 8 it is seen that a uniform reduction of the incident electron energies by 7% would be unacceptable. Such a reduction would make the differences between the calculated and measured values of $\%dd(10)$ and TPR^{20}_{10} values at 4 MV unacceptably large and would make the agreement of all heavily-filtered beams and most lightly-filtered beams worse. Overall such a reduction would also make the agreement with measurements worse although at isolated beam qualities (*e.g.* 12 MV lightly filtered) it would probably improve agreement.

Using the $\%dd(10)_{\mathsf{x}}$ beam quality specifier, Figure 12 shows that the k_Q values for the lightly and heavily filtered beams at the NPL produce a single curve (except for the lightly-filtered 4 MV beam). In contrast, when TPR^{20}_{10} is used as a beam quality specifier there are 2 distinct curves. This result strongly suggests that $\%dd(10)_{\mathsf{x}}$ is a better beam quality specifier than TPR^{20}_{10}.

8 Acknowledgments

We wish to thank our colleagues at NPL who have generously answered an endless stream of questions with patience. In particular we thank Simon Duane, David Shipley, Alan DuSautoy, Karen Rosser and Rebecca Nutbrown. We also thank Richard Knight who sent us extensive information several years ago. Thanks also to our NRC colleague, Jan Seuntjens for many helpful discussions.

9 References

[1] X. A. Li and D. W. O. Rogers. Reducing Electron Contamination for Photon-Beam-Quality Specification. *Med. Phys.*, 21:791 – 798, 1994.

[2] A. Kosunen and D. W. O. Rogers. DDSPR: A Code for calculating photon beam depth-dose curves and stopping-power ratios for an arbitrary spectrum. *National Research Council Canada Report PIRS-298*, 1992.

[3] A. Kosunen and D. W. O. Rogers. Beam Quality Specification for Photon Beam Dosimetry. *Med. Phys.*, 20:1181 – 1188, 1993.

[4] A. S. Kirov, D. W. O. Rogers, G. M. Daskalov, and J.F. Williamson. Secondary electron transport in brachytherapy dosimetry: Evaluation of the dose-to-kerma ratio for localized gamma sources. *Medical Physics*, 23:1056(abstract), 1996.

[5] D. W. O. Rogers, B. A. Faddegon, G. X. Ding, C. M. Ma, J. Wei, and T. R. Mackie. BEAM: A Monte Carlo code to simulate radiotherapy treatment units. *Med. Phys.*, 22:503 – 524, 1995.

[6] R. T. Knight. Absorbed dose conversion factors for therapeutic kilovoltage and megavoltage x-ray beams calculated by the Monte Carlo method. *PhD Thesis, University of London, UK*, 1996.

[7] D. W. O. Rogers, C. M. Ma, G. X. Ding, B. Walters, D. Sheikh-Bagheri, and G. G. Zhang. BEAM98 Users Manual. *NRC Report PIRS 509(a)revC*, 1998.

[8] C. L. Yang, D. W. O. Rogers, and J.P. Seuntjens. Calculation of photon beam quality specifiers. *Proceedings of the 1998 COMP Annual Meeting (Canadian Organization of Medical Physicists, Edmonton, Alberta)*, pages 186 – 188, 1998.

[9] D.S. Followill, R. C. Tailor, V. M. Tello, and W. F. Hanson. An empirical relationship for determining photon beam quality in TG-21 from a ratio of percent depth doses. *Med. Phys.*, 25:1202 – 1205, 1998.